Available online at www.sciencedirect.com
ScienceDirect
Focus Article, *Mendeleev Commun.*, 2016, **26**, 177–186
Mendeleev Communications

Nanostructured silver materials for noninvasive medical diagnostics by surface-enhanced Raman spectroscopy

Anna A. Semenova,[a] Alexander P. Semenov,[b] Elena A. Gudilina,[c] Galina T. Sinyukova,[c] Nadezhda A. Brazhe,[d] Georgy V. Maksimov[d] and Eugene A. Goodilin*[a,e]

[a] *Department of Materials Science, M. V. Lomonosov Moscow State University, 119991 Moscow, Russian Federation. Fax: +7 495 939 0998; e-mail: goodilin@inorg.chem.msu.ru*
[b] *Institute of Physical Materials Science, Siberian Branch of the Russian Academy of Sciences, 670047 Ulan-Ude, Russian Federation*
[c] *N. N. Blokhin Russian Cancer Research Center, 115478 Moscow, Russian Federation*
[d] *Department of Biology, M. V. Lomonosov Moscow State University, 119991 Moscow, Russian Federation*
[e] *Department of Chemistry, M. V. Lomonosov Moscow State University, 119991 Moscow, Russian Federation*

DOI: 10.1016/j.mencom.2016.04.001

Noninvasive medical diagnostics as a modern research and application trend faces with a key problem of successive development of novel materials. Recently, new powerful approaches based on surface-enhanced Raman spectroscopy have become incredibly popular since they promise a unique analysis of biochemical processes on cell, cell organelle and molecular levels. Silver nanostructures and composites are preferred for such an analysis because of easier and more flexible preparation ways, better affinity to biological species, extraordinary spectral sensitivity and a wide variety of morphological forms of silver nanomaterials.

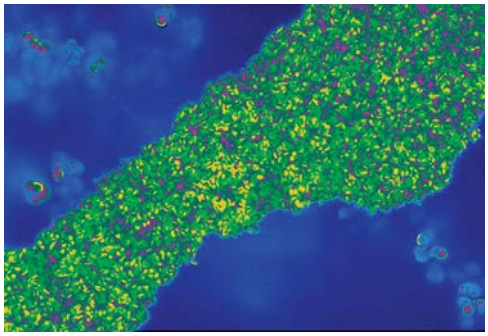

Anna A. Semenova, PhD in chemistry, Department of Materials Science, M. V. Lomonosov Moscow State University; scientific interests: novel preparation techniques of nanostructured silver materials.

Elena A. Gudilina, PhD in medicine, N. N. Blokhin Russian Cancer Research Center; scientific interests: ultrasound diagnostics and contrasts.

Nadezhda A. Brazhe, PhD in biology, Department of Biology, M. V. Lomonosov Moscow State University; scientific interests: cell biology and SERS studies.

Eugene A. Goodilin, Dr. Sci., Professor, Department of Materials Science, M. V. Lomonosov Moscow State University; scientific interests: nanochemistry and solid state chemistry.

Alexander P. Semenov, Dr. Sci., Professor, Director of the Institute of Physical Materials Science, Siberian Branch of the Russian Academy of Sciences; scientific interests: plasma physics and electronics.

Galina T. Sinyukova, Dr. Sci., Professor, Head of ultrasound diagnostics sector, N. N. Blokhin Russian Cancer Research Center; scientific interests: modern ultrasound diagnostics.

Georgy V. Maksimov, Dr. Sci., Professor, Deputy head of biophysics chair, Department of Biology, M. V. Lomonosov Moscow State University; scientific interests: neural cells and SERS.

Classical methods of noninvasive medical diagnostics include mostly X-ray computer tomography, ultrasound tomography, scintigraphy, SQUID (superconducting quantum interference device) magnetometry, magnetic resonance tomography, positron emission tomography;[1–5] some of them require new nanomaterials – like ultrasound or computer tomography contrasts – to provide useful information taken for diagnostics. Modern noninvasive medical diagnostics for screening and personal medicine admit a challenge of highly sensitive single molecule or single cell analysis and thus demand thorough development of innovative materials and novel analytical approaches. In this context, Raman scattering spectroscopy is especially suited for the detection of various molecule fingerprints, biomolecule conformation and interactions in biological samples, even in living cells, virus, deoxyribonucleic acid (DNA), because of a negligible influence of fluorescence and interference from water.[6,7] However, natural concentrations of molecules of interest in living cells are usually much lower than the detection limit of conventional Raman scattering spectroscopy. Surface-enhanced Raman spectroscopy (SERS) could solve this problem since the signal can be enhanced by many orders of magnitude.[8,9] SERS combines molecular fingerprint specificity and, potentially, single-molecule sensitivity. These features make SERS a promising low-cost and real-time tool for biomedical applications.[9–20] Noble metals like silver and gold are commonly used to attain large enhancement factors in SERS as achieved by varying nanoparticle sizes, shapes and aggregative structures.[11–13,21–27]

Unfortunately, SERS of biomolecules still suffers a lack of reproducibility due to possible toxicity of metallic nanoparticles, masking SERS signals by surfactants or by-products, gradients of electric fields near the nanoparticles and variations of biomolecule positions with respect to the nanoparticles.[16,28–30] Commonly used linkers, surfactants, reducing agents and their oxidized forms, halide ions *etc*. can affect biomolecules, prevent a target molecule to approach a close proximity of nanoparticles or change characteristic properties of nanoparticles because of their aging, recrystallization or random formation of aggregates. Nanostructured substrates promise much better reproducibility and less toxicity promoting their SERS applications in biology and medicine, especially in highly sensitive lab-on-a-chip devices.[16,17,31–33] The latter opens up perspectives for rapid monitoring of living cells and their organelles. Superficial roughness of the substrates can be created by deposition of metal colloids onto surfaces, vapor deposition of metals, nanocasting and lithography, electrochemical deposition through a template of self-assembled latex spheres, abridging pillar tip spacing by sputtering, self-assembly of large-scale and ultrathin nanoplate films, application of porous substrates.[17,31–33] A problem of noble metal toxicity is still being discussed in the literature[6,7,34–38] as well as mechanisms of Raman signal amplification which seems to be unique for biological objects. This set of factors demands new approaches of future single-molecule, single-cell or single-organelle medical diagnostics as discussed in this short review.

Key advantages of silver and morphological variety of nanostructures

Silver nanoparticles and nanostructured materials attract sustained interest in various applications due to their fascinating biological activity, a great potential as catalysts, sensing materials or building blocks for nanoscale devices. Silver nanoparticles have proven to be a common choice for SERS measurements due to their broad plasmon resonance, high stability, facile fabrication methods and the most exciting 10^{10}–10^{14}-fold enhancement for special molecules.[21–27] A complex morphology such as nanoflowers, nanorices, cubs, multipods and nanodendrites, mesocages is achieved by kinetically controlled, aggregation-based, heterogeneously seeded,

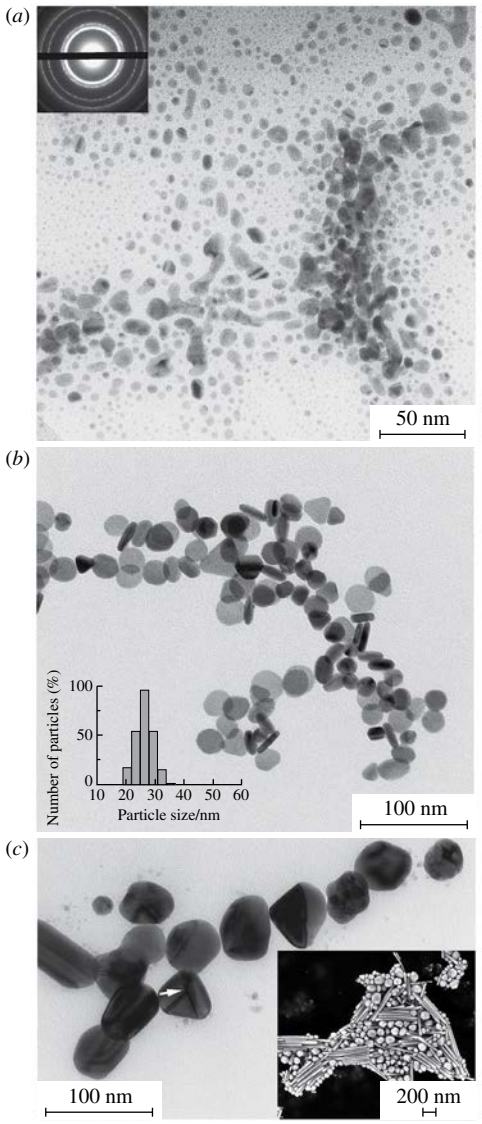

Figure 1 Silver nanoparticles prepared by different methods (micrographs of authors): (*a*) preparation of pure silver hydrosols of isotropic nanoparticles from diamminesilver hydroxide, (*b*) PVP-stabilized plate-like silver nanoparticles by seeding and anisotropic growth method, (*c*) polyhedral and wire-like silver nanoparticles by the polyol preparation route.

template-directed growth, selective etching and colloidal system aging, the polyol technique allows one to synthesize silver nanoparticles of a wide variety of shapes and sizes (Figure 1).[9,12,16,21,34-60]

Most of these methods produce colloidal systems being not compatible with biological objects and this lack of compatibility of traditional preparation techniques demands for new precursors. In particular, pure silver nanoparticles (AgNPs) are expected to form if a preparation method uses the components of a 'water–silver' system only; it means that silver(I) oxide is consistent perfectly. This compound introduces silver and oxygen solely, the reduction of Ag_2O occurs easily in water environment, finally, Ag_2O is not soluble in water therefore it can be easily produced, separated and purified by simple washing. At the same time silver(I) oxide can be dissolved by aqueous NH_3 which is volatile and can be removed from the solution by boiling. Silver(I) oxide was applied to form silver nanoparticles by reduction with hydrogen peroxide, gaseous hydrogen or poly(*N*-vinyl-2-pyrrolidone).[39] However, a question remains if there is a simpler way to produce nanoparticles without special reducing agents, salts, stabilizers or anionic pollutants. We consider a simple and effective way supported by our previous works,[61–73] which is based on gradual self-reduction of one of well-known ammonia complex of silver,

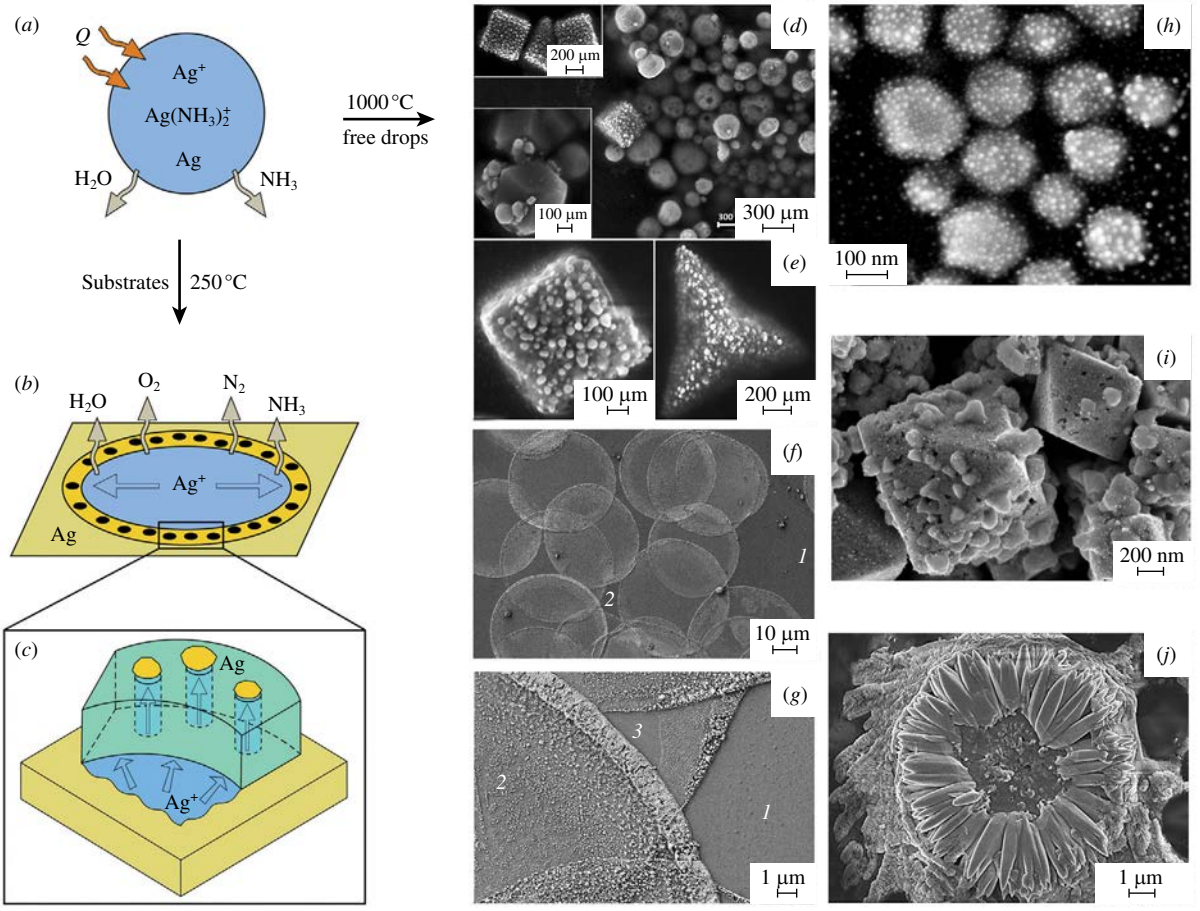

Figure 2 A wide variety of morphological types of silver nanostructured materials prepared from silver amino complexes under different conditions (micrographs of authors): (*a*) schematic drawing of aerosol droplets of aqueous diamminesilver hydroxide, (*b*) aerosol deposition process forming 'coffee ring' silver nanostructures of hierarchically structured substrates and diagnostic chip prototypes using the USSR procedure, (*c*) porous structure of silver ring craters, droplets forming pure silver rings on a preheated substrate with an additional effect of silver crater wall formation, silver-containing liquid spreads over the substrate, penetrates upward through a porous silver wall to form 'sesame seed' nanocrystals of silver on the top of the wall, (*d*), (*e*) porous superficially decorated silver cubes formed under high decomposition temperatures, (*f*), (*g*) coffee ring silver nanostructure after aerosol droplet decomposition on warm substrates under mild conditions, a general SEM image; (*f*) (*1*) a flat area coated with separate clusters of AgNPs coming from a spreading liquid film, (*2*) intersecting circles ('craters'), a magnified view; (*g*) (*1*) separate silver clusters, (*2*) a gradually increased population of silver clusters inside a ring, (*3*) a silver wall contouring an evaporated droplet of the silver(I) complex; (*h*) pollen-like superficially decorated polyhedral silver nanoparticles; (*i*) octahedral pseudomorphs (AAS, unpublished data); (*j*) flower-like particles.

$[Ag(NH_3)_2]^+$, due the lost of its stability upon the ammonia ligand leakage (Figure 2).

This route utilizes drastic stabilization of silver ions within the complex ($K_{stab}([Ag(NH_3)_2]^+) = 1.3\times10^7$, $Ag^+ + 2NH_3 = [Ag(NH_3)_2]^+$), huge variation of the redox potential $E^0_{Ag/Ag^+} = 0.8$ V in the presence of ammonia, a possibility to precipitate the Ag_2O solid phase or dissolve it by ammonia ($Ag_2O + H_2O + 4NH_3 = 2[Ag(NH_3)_2]^+ + 2OH^-$) and, finally, the absence of side anions in the redox system except OH^-, which is a natural part of all the aqueous solutions ($K_w = [H^+][OH^-] = 10^{-14}$). Another part of the system is oxygen which can be dissolved in the solution as an oxidizing agent or evolved from the solution as a product of silver oxide decomposition ($E^0_{O_2}/OH^-$ = 0.401 V). The overall reaction $Ag + {}^1/_4O_2 + 2NH_3 = [Ag(NH_3)_2]^+ + OH^-$ serves as a good control tool for generation of silver nanoparticles simply by changing the concentration of ammonia, which could generate enough Ag^+ ions to cause their reduction to metallic silver, otherwise Ag^+ is stabilized as $[Ag(NH_3)_2]^+$ and cannot be reduced.[63–65,69,70]

A thermal treatment of ultrasonic mists of this silver complex provides irreversible decomposition and solvent evaporation. The products of this transformation include silver nanostructured particles, water, ammonia and oxygen. Quenching of such products yields nanostructured particles and their aggregates formed in a shock manner, since the whole transformation occurs for few seconds at high temperatures.[67] High-temperature silver microspheres of about 100 nm in size are typical of aerosol spray pyrolysis because of solvent evaporation from mist droplets and spontaneous formation of silver nuclei joining into a porous 'orange skin' layer. Polyhedral aggregates formed could be a consequence of primary silver(I) oxide formation within the mist droplets prior to its decomposition. The process results in cubic, edge- and corner-truncated cubic, rhombicuboctahedral, edge- and corner-truncated octahedral, octahedral, and hexapod structures[13] and they could transform into pure silver forming pores due to oxygen liberation. The metallic silver cuboids could be considered as pseudocrystals formed in a topotactic manner preserving the shape of precursor crystals of silver(I) oxide (Figure 2).

Silver ring structures caused by the known 'coffee ring' effect are formed at moderate temperatures of 200–250 °C due to deposition of the mist droplets onto a preheated substrate (Figure 2). The coatings consist of overlapping silver rings of a complex morphology originated from decomposition of micrometre-sized droplets of ultrasonic mist of silver(I) solution. This resembles a rain making rings on a flat dusty surface, hence, we call it Ultrasonic Silver Rain (USSR). Usually, silver deposition gives intersecting circles of 30–100 μm in diameter.[69] This value is several times larger than the expected size of 1–10 μm of the falling mist droplets as occurred because the liquid from the droplets spreads laterally over the substrate. Solvent evaporation increases

concentration of the silver complex and then metallic silver resides on rims of the spreading circles producing walls of silver craters. The thickness of walls lies typically in a range of 1–3 μm, while the residual part is covered with sparse silver nanoclusters gradually increasing in their sizes from 10–20 nm in the centers of circles to about 100 nm in the wall vicinities. The nanoclusters increase the role of capillary forces and, afterwards, more droplets stack onto the surface, boil, decompose, even 'explode' producing hollow silver 'coconuts'; an increase of sputtering time leads to rough and porous layers. This deposition mode has several advantages in terms of manufacturing SERS-active structures for promising applications:[62,69] silver micro- and nanostructures are immobilized onto a substrate and form a rather stable metallic film on cheap materials like glass, there is no need to filter or separate nanoparticles, the nanostructure consists of porous silver sponge only, the temperatures are high enough for the one-stage formation of metallic silver.[66]

Superficially decorated pollen-like silver nanoparticles[64] were also prepared by a two-step procedure including the formation of original silver nanoparticles as carriers of smaller nanoparticles followed by *chimie douce* superficial decoration (Figure 2). Round-shaped and wire-like nanoparticles were prepared by the polyol method.[57] As reported,[74] formation and growth of silver nanowires may be caused by the deposition of silver atoms on {111} planes. These facets are atomically rough compared to the flat {100} grains, that is why supersaturation relaxes in the course of polyol process by fast deposition of adatoms onto these particular grains providing highly anisotropic growth of the fibers. The twinned silver nanowires could thus arise from a selective interaction between the polyvinylpyrrolidone (PVP) molecules and {100} planes. The clusters decorating the surface of original silver nanoparticles range their size within 5–50 nm. That is typical of a continuous nucleation and growth process, in which new nuclei are formed, while old ones increase their size in time. Such a pollen-like morphology manifests silver reduction and re-deposition from the dissolved $[Ag(NH_3)_2]^+$ ions.

Such a morphology could be caused by step-by-step metallic silver oxidation with molecular oxygen due to silver(I) stabilization within its ammonia complex, the complex accumulation as an intermediate product and its consecutive gradual decay into nanosilver in a redox reaction of silver(I) decreasing its overall concentration in time. This is an intriguing example of an interplay of redox potentials of bare silver(I) cations and those in the ammonia complex. Thus, superficially decorated silver nanoparticles are obtained in the course of aging of silver globules and fibers as soon as both aqueous ammonia and air are supplied.

One known criticism of silver as a SERS material is related to its oxidation in open air. However, recent results seem to show better stability of chemically produced nanostructures making chemical routes more attractive. Indeed, a known feature of silver is its special ability to dissolve oxygen even at room temperature, in some reported cases, this process results in degradation of its properties; in particular, it is found that oxygen interaction with silver nanoparticles depends strongly on their size, an increase in size leads to formation of oxide-like species followed by covering of metallic silver by Ag_2O thin layers as facilitated by extended defects.[75–81] The chemical bonding of oxygen species on small particles differs from that on 'bulk' silver surfaces.

Two types of chemically prepared and physically deposited samples were taken into consideration[81] including those freshly prepared within a day or a week and others stored for 11–12 months in environmental air. Based on X-ray photoelectron spectroscopy (XPS) of the samples, we found that the chemically deposited layers preserved their high SERS enhancement for a year, while the physically deposited (magnetron sputtered) samples demonstrated a gradual decrease of SERS properties already after a

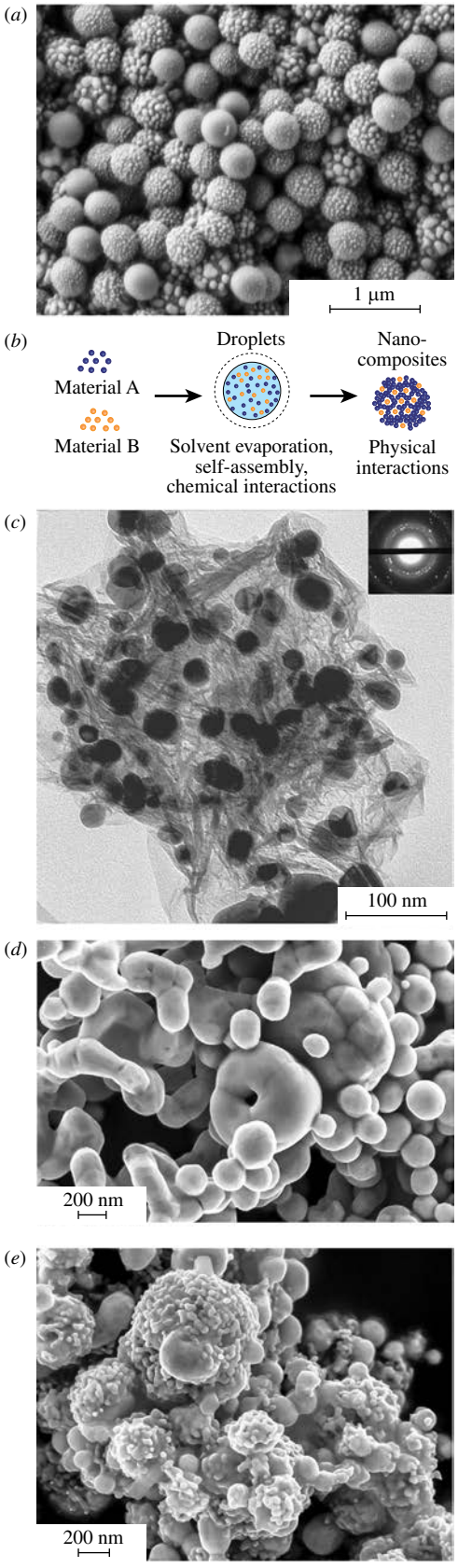

Figure 3 Prospective silver-based biocompatible nanocomposites prepared by modified ultrasonic aerosol spray pyrolysis (micrographs of authors): (*a*) silica beads decorated with silver nanoparticles, (*b*) a schematic drawing of the material formation, (*c*) graphene oxide-based nanocomposites loaded with silver nanoparticles, (*d*) pure silver nanoparticles, (*e*) magnetic Fe_3O_4–Ag nanocomposite. Preparation of SERS-active nanocomposites using the proposed carriers of silver nanoparticles results in quite different optical properties which allow one to differentiate the materials in terms of their practical applications.

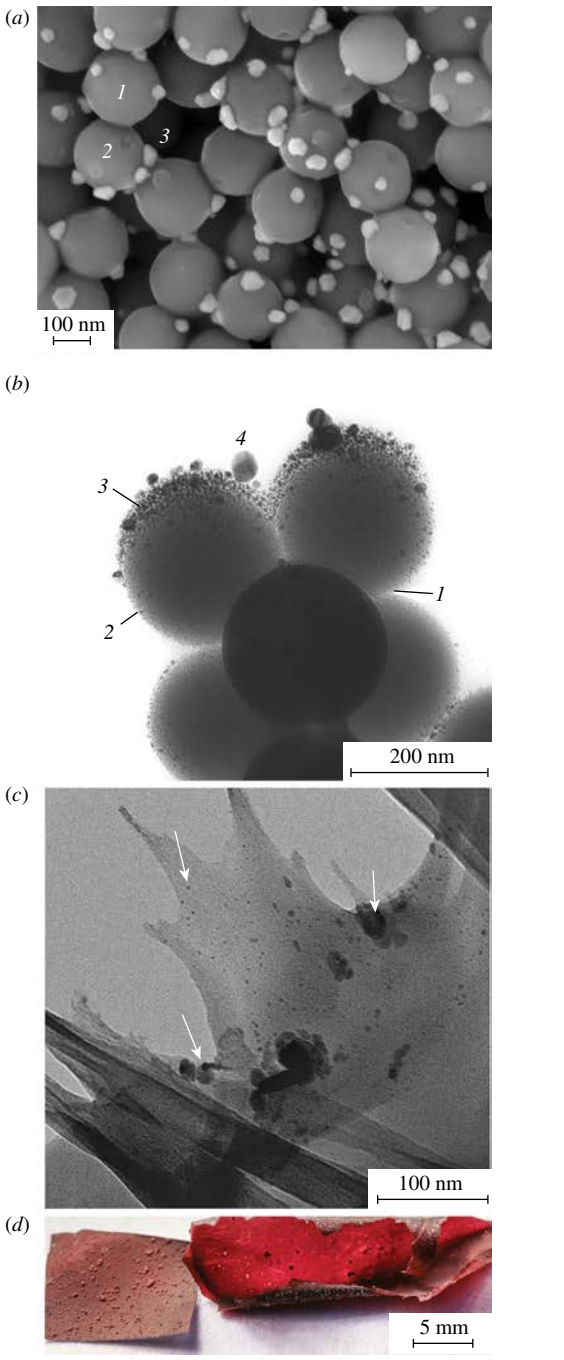

Figure 4 Silver-based biocompatible nanocomposites prepared by soft chemistry and physical methods (micrographs of authors): (*a*) Microstructural features of silver–Stöber silica composites based on seeding and regrowth technique showing (*1*) silica beads, (*2*) pits on the surface of silica and (*3*) polygonal silver nanoparticles; (*b*) silver ion sputtering on silica beads (*1*) when forming (*2*, *3*) small silver clusters and (*4*) larger silver nanoparticles; (*c*) mixture of silver nanoplates of different aspect rations on cellulose substrate; (*d*) sacrificial polymer films containing silica beads with polygonal silver nanoparticles.

month of storage. XPS studies confirmed that the surface of magnetron sample was contaminated with oxygen derivatives of carbon, the sample with a chemical prehistory prepared in the atmosphere of water vapor and ammonia contained no nitrogen, although magnetron deposited samples demonstrated nitrogen valence states likely corresponding to nitrides or oxynitrides.[69]

Simple easy-to-prepare sols of noble metal nanoparticles are popular in SERS investigations.[6,9,11,16,18] However, despite of all possible advantages, the nanoparticles themselves are likely to aggregate uncontrollably in solutions making it difficult to reproduce SERS results. Nanoparticle sols exhibit also limited plasmonic tuneability as compared to a new class of nanomaterials – colloidosomes (Figures 3 and 4) composed of a dielectric core and a concentric metal shells with hybridization of plasmon modes supported by an inner cavity and an outer surface of the nanoshell.[82–90] The colloidosome family of SERS nanocomposites makes it possible to tune plasmon resonance bands readily by the size of the cores, the thickness of the metal shells, the dielectric core coverage with plasmonic nanoparticles, the coupling between neighboring particles and the appearance of additional 'hot spots'. In particular, one effective strategy to design SERS-active materials is based on preparation of nanocomposites composed of microparticles, like Stöber-derived silica microbeads, decorated with nanoparticles.[84–90]

Such materials allow one to concentrate nanoparticles on the surface of dielectric microcarriers, organize additional hot spots, build up self-assembling structures and control optical properties by varying the thickness and coverage of the SiO_2 core by the silver shell. Usually, silver reduction agents like ascorbic acid, $NaBH_4$, Sn^{II}, PVP are used to produce and electrostatically attract silver nanoparticles to the surface of silica, while it is shown in a number of recent papers that diamminesilver(I) complexes can be used to produce silver nanoparticles under mild conditions.[61,63] In such a case, a typical size of the isotropic silver nanoparticles embedded (encrusted) into the superficial layer of silica is surprisingly small, only about 2–5 nm, and demonstrates no large deviation in the mean size. It seems that an etching process is important for further overgrowth of silver since many originally formed seeding nanoparticles go deeply into the body of silica microspheres, they are encrusted into the superficial layer. An additional overgrowth step can result in unusual facetted platelike nanoparticles (Figure 4).[63] Physical deposition techniques result in Janus particles (Figure 4) with round shaped particles, while preparation of anisotropic silver nanoplates allows one to deposit them onto biocompatible cellulose substrate making it SERS-active with enhanced spectral sensitivity (Figure 4). In addition, the resulting nanocomposites are reasonable to store inside a sacrificial biopolymer film like hydroxyethylcellulose[63] which is a good candidate as a carrier of nanoparticles that could prevent environmental damage of the nanoparticles and also make it suitable to apply the material for an advanced SERS analysis. A wide shoulder of light absorption of such nanocomposites allows one to apply different laser irradiations to agitate Raman signals. The samples are SERS-active and exhibit a new example of robust and flexible technology to produce biocompatible SERS materials with adjustable functional properties (Figure 4).

Biological objects and silver nanomaterials

A recent trend of SERS applications demands an enhancement of Raman scattering of molecules separated from nanoparticles by a certain structure (for example, cell membranes, Figure 5). That is desired for studies of biomolecules in their natural environment in cells or organelles.[61,62,69] The nanocomposites like colloidosomes allow one to concentrate nanoparticles on the surface of dielectric microcarriers, build up self-assembling structures, reduce possible toxicity effects with respect to biological objects, caused otherwise by free nanoparticles, and provide multifunctionality by introducing biocompatible, magnetic, mesoporous and other cores with varied optical properties. This unique set of abilities makes colloidosomes to be excellent candidates for biology-oriented SERS, however, the problem remains challenging especially for intact organelles[62] in the course of noninvasive monitoring of their functions. It is important to understand that, in the case of single molecules, the enhancement of Raman signal occurs due to, at least, several known reasons, including a local electrical field amplification, a charge transfer between nanoparticles and the molecules and 'hot spot' forma-

tion.[6–9] It is commonly considered that intense SERS spectra with well-defined peaks can be observed mostly for molecules that are attached to plasmonic nanostructures. Importantly, as soon as we consider molecules inside living cells, no physical contact between nanoparticles and the analyte molecules is possible. Obviously, both the 'hot spot' and the charge transfer enhancement vanish in this case since they require a close contact between the molecules and the nanostructures. Therefore, the remaining electromagnetic field enhancement becomes a dominant mechanism, however, it is mostly determined by the morphological features of the nanostructured surface.

SERS studies of cells or cell organelles become a growing trend.[11,17,18,61,62,65,68,69,91–102] Most of fundamental and diagnostically oriented studies of cells and isolated biomolecules are done by SERS with silver or gold colloids. However, as mentioned above, they can be cell toxic, can change osmolarity of the cell environment, distribute inside the cell or on the cell surface non-evenly and can aggregate altering Raman enhancement. In this sense, nanostructured surfaces have several advantages, since they are more stable, do not contain preparation by-products and can give reproducible Raman enhancement.[61,62] An important application of SERS in biomedical diagnostics involves studies of hemoglobin (Hb) abnormalities caused by erythrocyte malfunction as a result of pathologies of the cardiovascular system or key organs.[11,61,65,68,69,91–96] Unfortunately, Hb itself points to a general problem related to the SERS analysis of biomolecules. As soon as Hb is leaked from an erythrocyte, it might interact with colloidal nanoparticles, they tend to attach to heme, tryptophan, amide and aromatic amines, cause conformational changes, unfolding, formation of charge-transfers complexes and, finally, sedimentation of large aggregates. These circumstances urge the development of new experimental approaches to study undisturbed structures of Hb in its natural cellular environment to provide the analysis of these important cells 'as is'. SERS studies of blood are disappointingly rare.[11,61,65,69,96] The substrates with hierarchic 'coffee ring' morphology[69] evoke no hemolysis, they are suitable to immobilize erythrocytes, provide a tight contact of the silver nanostructure with erythrocyte membranes. As a result, SERS from submembrane hemoglobin (Hb_{sm}) inside single living erythrocytes was observed confirming effectiveness of such a morphology for the design of biosensor chips. In principle, each living erythrocyte contains two distinct populations of Hb molecules including cytosolic (Hb_c) and submembrane (Hb_{sm}) hemoglobin bound to the cytosolic domain of the membrane anion exchanger AE1 and located no deeper than 15–20 nm from the extracellular surface of erythrocytic plasma membrane (Figure 5).[69] In traditional Raman spectroscopy, spectra of erythrocytes correspond to Raman scattering of Hb_c since the contribution of Hb_{sm} is negligible because of its very low concentration of less than 0.5% of Hb_c. However, it should be Hb_{sm} that contributes mostly to the enhancement of Raman scattering since it is located much closer to the contacting silver nanostructures.[69] It is the right choice to analyze Hb_{sm} since the functional state of membrane bound Hb_{sm} is highly relevant to the understanding of red blood cell regulatory processes, hemoglobinopathies and, then, possible medical diagnostics.

Mitochondria are organelles of fundamental importance for cellular energy production, metabolic regulation, aging and cell survival under stress (Figure 5).[61,62,103–117] A normal function of mitochondria and their pathological changes, including production of reactive oxygen species (ROS), are heavily dependent on the redox state of the electron transport chain (ETC) cytochromes and cytochrome *c*, in particular. At present, most of studies of isolated mitochondria and mitochondria in cells are performed by fluorescent microscopy, absorption spectroscopy and measurements of O_2 consumption. The fluorescent microscopy with small fluorescent dyes or fluorescent proteins can provide general information about changes in the potential of the inner mitochondrial membrane, the mitochondrial volume, and the co-localization of certain mitochondrial components with a molecule of interest. In spite of numerous advantages, these methods provide only indirect information about the redox state of ETC complexes. The direct information about cytochrome *c* redox state and its intermembrane space (IMS) dynamics in living mitochondria is still difficult to obtain since they are highly dynamic, affecting cytochrome diffusion in IMS, interaction with complexes III and IV and the electron transfer. Thus, a sensitive, noninvasive, label-free analysis of cytochrome *c* inside intact

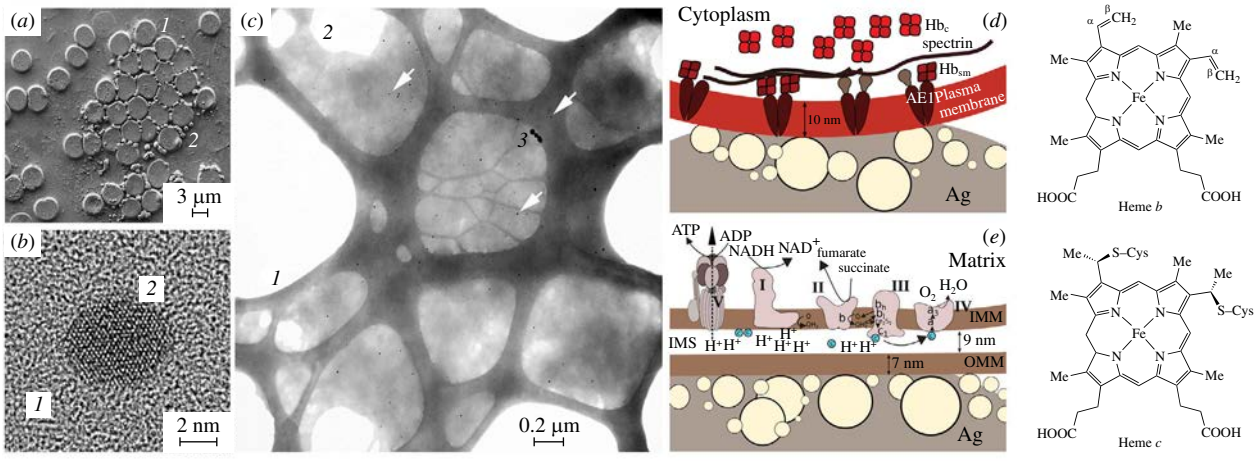

Figure 5 Interaction of silver nanoparticles with cell membranes. (*a*) A general view of erythrocytes mixed with silver hydrosol, (*b*) a TEM image of a part of erythrocyte membrane (*1*) with a small silver nanoparticle (*2*), (*c*) a general view of erythrocyte ghosts mixed with silver hydrosol, (*1*) an edge of TEM mesh, (*2*) the edge of erythrocyte membrane (host), (*3*) large silver nanoparticles onto the membrane, smaller AgNPs are marked with arrows, (*d*, *e*) red blood cells and mitochondria studied by SERS. (*d*) A scheme of a submembrane region of an erythrocyte contacting with SERS-active silver nanocomposite, a 10 nm thick cell membrane. Hb_{sm}, Hb_c – molecules of the submembrane and cytosolic hemoglobin (Hb), respectively; AE1 – an anion exchanger binding Hb and the ankyrin protein that together with the spectrin forms a submembrane cytoskeleton. (*e*) A scheme of outer and inner mitochondrial membranes (OMM and IMM, respectively) with the complexes I–V of the electron transport chain (ETC). Cytochromes of *a*, *b* and *c*-types are shown by the letters 'a', 'b' and 'c' in the corresponding complexes. The cytochrome *c* is shown as cyan balls diffusing in the intermembrane space (IMS) and interacting with complexes III and IV. The black numbers with arrows in both the figures indicate an approximate thicknesses of the erythrocytic plasma membrane, the outer mitochondrial membrane and intermembrane space. The distance between the outer and the inner membranes of mitohondria varies around 10 nm depending on many factors, including a matrix volume, activity of the ATP synthesis and IMS amount of ADP, the number of contact sites between the outer and inner mitochondrial membranes. The right insets demonstrate structural formulas of heme *b* in hemoglobin and cytochrome *b* molecules and heme *c* in cytochromes *c* and *c*1.

functional mitochondria can extend our understanding of the role of cytochrome *c* in the modulation of ETC activity and the development of mitochondria pathologies.[61,62] Raman scattering of cytochromes is sensitive to their redox state, mitochondrial membrane potential and the activity of electron transport.[61,62,107–112] Previously, SERS spectra were recorded from purified oxidized or reduced cytochrome *c* adsorbed on silver electrode or mixed with silver colloid. Both reduced and oxidized cytochromes possess intensive SERS spectra and can be distinguished from one another. However, there are only a few reports on SERS and TERS observation of isolated mitochondria.[61,62,116,117]

We demonstrated recently that it is possible to enhance Raman scattering of *c*-type cytochromes in ETC of functional living mitochondria by means of specially designed silver nanostructured substrates or colloidosomes[61,62] and that the SERS spectra of mitochondrial cytochrome *c* are sensitive to the H^+-gradient across IMM, mitochondrial membrane potential and the ATP synthesis. The limitation of the proposed approach is that it can be used to study cytochrome *c* in isolated mitochondria, not in mitochondria in cells, since nanostructured surfaces cannot be endocytosized. Thus, mitochondria remain challenging but highly desired objects for SERS and this reveals common trends in SERS biomedical diagnostics in searching for oncomarkers, analyzing the effects of new pharmaceutical agents, looking at chemical processes inside embrions, for viruses, important cells and organelles.[6,7,9,11,14,37]

Practical approaches on SERS diagnostics of biological objects

Practical implementations of SERS active nanomaterials often face additional problems, including a demand of enhancement of spectral sensitivity, necessity to reduce noise and background signals, increasing reproducibility of SERS measurements. Note that an ensemble of traditionally used spherical particles gives no broad extinction spectra contrary to those observed experimentally since isotropic nanoparticles possess a narrow plasmon peak and, moreover, this narrow peak is red-shifted only by 15–20 nm even if the particle size becomes several times larger.[8–10,64,68,73] Figure 6 confirms this, indicating that the peak of small spherical particles is located at about 400 nm, and much larger, almost isotropic 40×40×48 ellipsoids have two peaks at about 405 and 425 nm, therefore, even a small anisotropy gives already a contribution to the red-shifted part of the overall extinction spectra. It is ambiguous to correlate strictly the SERS enhancement and the plasmonic band position because the influence of small nanoparticles seems to be the most important for SERS. Thus, optical features demonstrated by ensembles of silver nanoparticles (Figure 6) make us to believe that a mean particle size and complexity of the morphology is not the only reason of usually observed broad plasmonic peaks but it is particle size distribution peculiarities that contribute substantially to the overall SERS enhancement parameters.

Artificial nanoparticle mixtures and aggregates are, in principle, favourable for an advanced design of universal substrates for a SERS analysis of living cells. Indeed, if several different nanoparticles are present onto an area of several microns, as small as typical dimensions of cells, there are at least some of them contributing greatly to the Raman enhancement because a laser irradiation wavelength, a suitable plasmon band position and an absorption range of analyzing molecules coincide with each other. There is no sense to create 'hot spots' or other constructions for 'single-molecular' detection since they cannot operate due to a thick cell membranes and a large size of cells. That is why a local electromagnetic field remains effective only in the case of non-invasive transmembrane analysis of living cells. The same principle is valid for stochastic silver ring structures or nanoparticles of a complex shape demonstrating light absorption in a wide range due to the presence of elements of different scales.[61–65,69] At the same time preparation of such substrates for biosensor chips[69] guarantees that the nanomaterials produced are safe for biological objects and *vice versa*.

A wide range of different materials as nanoparticle carriers could be hypothetically suitable for transmembrane SERS studies of these important biological objects but their real applications require some additional features like high chemical stability, biocompatibility, nanoparticle bonding ability and also the materials should not have their own Raman peaks being enhanced by nanoparticles and thus disrupting the final spectral data. Such

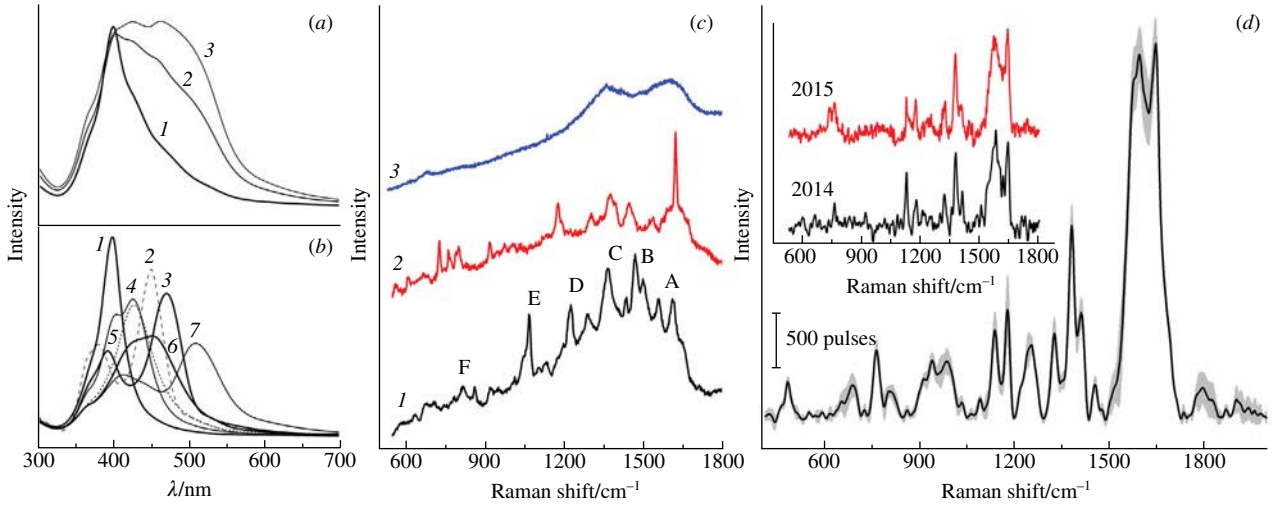

Figure 6 Optical properties of biocolloids for SERS studies of cells and organelles. (*a*) Discrete dipole approximation of simulated extinction spectra of nanoparticle ensembles, plasmonic bands for mixed fractions of 70×70×105, 40×40×60, 70×70×84, 40×40×48 nm ellipsoids and 10 nm spheres with contributions (%) of (*1*) 10:10:10:30:50, (*2*) 35:10:35:10:10 and (*3*) 50:20:20:10:0, respectively. (*b*) Spectral components of the simulated spectra, (*1*) 10 nm and (*5*) 70 nm spheres, (*2*) 10×10×15 nm, (*3*) 40×40×60 nm, (*4*) 40×40×48 nm, (*6*) 70×70×84 nm and (*7*) 70×70×105 nm ellipsoids, respectively. (*c*) 'Background' Raman signals of as-prepared SiO_2 colloidosomes decorated with silver nanoparticles and with no analytes added, (*1*) Stöber SiO_2 microspheres, aqueous $AgNO_3$ reduction with $NaBH_4$, (*2*) Stöber-derived SiO_2 after drying at 500 °C, ultrasonication and borohydride coating with silver nanoparticles, (*3*) aerosol-derived SiO_2–Ag (streaming temperature 850 °C). (*d*) Reproducibility of SERS spectra of functioning mitochondria using Ag–SiO_2 colloidosomes: an averaged spectrum (thick black line) and standard deviations (grey area) for a series of spectra measured from either one and the same or different points. The inset shows two spectra measured using the same colloidosomal material but for different mitochondria series with a period of separate measurements of about one year.

signals are, indeed, negligibly small if the enhancement coefficient reaches 10^{10}–10^{14} for adsorbed cherry-picked model molecules, however, the absence of a SERS signal from nanoparticle carriers becomes important for the transmembrane analysis of living cells and organelles with the remaining 10^4–10^6 electromagnetic field enhancement. In particular, if a reaction of nanostructured silver formation occurs in aerosol droplets at high temperatures, then the final powder is not accompanied by side products and, thus, it requires short preparation time and no purification (Figure 6).[61] Therefore, the spraying process in the case of silica allows one to produce SERS-active silica beads coated with silver nanoparticles demonstrating a smooth background suitable for measurements of biological objects. Other standard preparation procedures of $Ag@SiO_2$ nanocomposites yield strong background signals. For example, peaks 'A' [Figure 6(*c*)] could be attributed to NH_2 groups, nitrates and/or C=C conjugated bonds, the 'B' group corresponds most probably to CH_2 deformation vibrations, 'C' accumulates CH_2 wagging–alcohol OH deformation vibrations, the 'D' group could correspond to nitrates, alcohol OH, CH_2 twisting or silica vibrations, small peaks 'E' and 'F' are Si–OH deformation, Si–O–Si and B–O bonds or Si–OH, Si–O–C (ethoxy) vibrations, respectively. Amino groups could appear due to aqueous ammonia used for TEOS (tetraethyl orthosilicate) hydrolysis, nitrates are the absorbed NO_3^- from silver nitrate being a source of silver nanoparticles remaining in the silver hydrosols. Thus room-temperature preparation or moderate annealing cannot yield a proper matrix for further silver nanoparticle deposition since SERS studies face numerous background peaks. Also, Si–OH groups are used as anchors in many traditional preparation methods to stick silver nanoparticles. The linkers could manifest themselves by bright vibration modes enhanced by silver nanoparticles and thus they might strongly interfere with possible analyte peaks. For example, a dominant intense line of PVP appears at 1606 cm^{-1} with a weak shoulder at 1660 cm^{-1}. Additionally, the CH_2 bending region is dramatically perturbed with the strongest line at 1380 cm^{-1}, PVP degrades under oxidizing conditions and form amorphous carbon. Such by-product peaks make it hard to apply traditional $Ag@SiO_2$ nanocomposites for an advanced analysis of biological objects. The reaction occurring in the course of pyrolysis results in pure $Fm\bar{3}m$ silver nanoparticles of 10–20 nm or their larger aggregates[61] deposited randomly on the surface of 250–300 nm SiO_2, while ammonia, oxygen and water are transferred into the gaseous phase and thus easily separated from the final $Ag@SiO_2$ colloidosomes by one-step aerosol pyrolysis. Different sizes of silver superficial aggregates originate of different volumes of aerosol droplets providing increased or decreased amounts of dissolved silver for each SiO_2 microsphere entrapped by a droplet of aqueous silver complex in streaming aerosol. Due to a sufficiently high concentration of silica colloid used for spraying, almost all the silver nanoparticles reside onto the surface of SiO_2 beads. The material could be stored, at least, for one year in our experiments preserving its functional properties and could be mixed on demand with different biological substances since all the silver particles are immobilized on the surface of silica microspheres, do not aggregate or change in time, also, the microspheres contain no biologically dangerous substances or surfactants and could be kept, in general, as an aseptic product.

USSR substrates demonstrate a negligible background.[65,68,69] This allowed us to use small laser power that prevented photo-induced damage of biological objects and ensured repeated measurements of SERS even from the same point.[69] SERS measurements of isolated Hb and erythrocyte ghost solutions (vesicles of erythrocytic plasma membrane without cytosolic Hb but with a different amount of Hb_{sm}) placed on the USSR substrates demonstrate that the observed SERS spectra correspond to Hb_{sm}. SERS spectra of living erythrocytes correspond to the enhanced scattering of Hb_{sm} and possess the same set of peaks as conventional Raman spectra of erythrocytes. Considering blood dilution and the amount of Hb_{sm} in erythrocytes, the enhancement factor for large peaks at 1370–1375 cm^{-1} in the SERS spectra is estimated[69] to be about 30 000. The latter means that our SERS experiments are relevant to a single-cell optical analysis.

SERS spectra of mitochondria (Figure 6) placed on the same substrate demonstrate[61,62] a set of intensive peaks corresponding to heme molecules of cytochromes of mitochondrial ETC with the position of their main maxima at 748, 1127, 1170, 1313, 1371, 1565, 1585 and 1638 cm^{-1}. These peaks originate from the normal group vibrations of pyrrole rings, methine bridges and side radicals in the heme molecule. The origin of SERS spectra of mitochondria comes from vibrations of the *c*-type heme in cytochrome, namely, the cytochrome *c*.[61,62] SERS spectra of reduced mitochondria correspond to SERS spectra of reduced purified cytochrome *c* and reveal a well-known shift of maximum positions of peaks sensitive to the redox state of Fe ion. We should note that ordinary Raman spectrum of mitochondria is noisy and does not contain Raman peaks of cytochromes even under high excitation power. SERS spectra of mitochondria recorded from different spots and from the same place repeatedly are highly reproducible.[61,62] Stability of mitochondria SERS spectra recorded from the same spot in time is an indicator of the absence of mitochondria photodamage under laser illumination. Intactness of mitochondria was determined using protonophores to check coupling between the electron transport and ATP synthesis. The coupling exists only in mitochondria with intact membranes and, therefore, mitochondria response to such agents is a good test on their integrity.[61,62] To demonstrate high sensitivity of SERS spectra of mitochondria to the proton gradient across IMM and mitochondrial membrane potential and to the redox state of other ETC complexes, we applied[61,62] protonophore FCCP and oligomycin as an inhibitor of ATP-synthetase (ETC complex V). FCCP-induced uncoupling of the electron transport and ATP synthesis leads to the decrease in the relative amount of reduced electron carriers including cytochrome *c*.[61,62] Oligomycin, to the contrary, due to the inhibition of ATP-synthase, causes accumulation of protons in the intermembrane space resulting in IMM hyperpolarization, decrease in the electron flow rate and the increase in the relative amount of the reduced electron carriers in ETC. The behavior of *c*-type cytochrome SERS peaks following FCCP and oligomycin treatments was in the complete agreement with the expected dependence of the reduction state of *c*-type cytochromes on the proton-motive force and the ETC loading with electrons.[61,62]

Cytochrome *c* is known to exist in several fractions (Figure 5): immobilized pool, bound to cardiolipin in the surface of internal mitochondrial membrane, mobile pool – 3D and 2D-diffusing cytochrome molecules moving in intermembrane space near or between inner and outer mitochondrial membranes and randomly interacting with ETC complexes III and IV and cytochrome molecules short-term bound to the complexes III or IV accepting or donating electrons. Under the ETC function, the distance between nanostructures and cytochrome *c* in mitochondria varies between 7–17 nm and can be greater if the intermembrane space thickness increases. The distance between cytochrome *c* bound to complex III and silver nanostructures is at least 13 nm. Cytochrome *c* bound to IMM or complex IV locates at ~17 nm from silver nanostructured surfaces. Relying on these data, we suppose that the SERS signal comes from 3D-diffusing cytochrome *c* and cytochrome *c* bound to complex III, while cytochrome *c* interacting with complex IV or cardiolipin of IMM does not contribute to SERS spectra. Colloidosomes demonstrate similar results.[61] Importantly, $Ag@SiO_2$ exhibits a high stability under prolonged

storage (Figure 6). Thus, SERS spectra of different mitochondria recorded using Ag@SiO_2 within the 11 month interval are very similar both in the spectral intensity and the set of peaks. This is an important finding since reproducibility and stability is a key issue for SERS materials.[118] The data indicate that the proposed SERS-based approach can be used to study conformational and redox state changes in cytochrome *c* in respiring isolated mitochondria under various conditions.

Thus, silver based nanomaterials demonstrate a great potential of their practical applications as SERS-based platform for biomedical studies approaching future medical diagnostics. Nanochemistry provides further new highly productive SERS-based tools for biomedical analysis.[119–127] An application of gold nanoparticles, minimally invasive to cells, gold nanopipettes for intracellular studies, development of novel TERS techniques adopted for biological objects reveal their extraordinary potential for biomedical diagnostics.[34] At the same time, a key problem of reproducibility of SERS results due to strong gradients of electric field around and between SERS nanoparticles and a variation of biomolecule positions with respect to the nanoparticles[118,126] require the further development of cost effective express techniques of optical noninvasive analysis. The rich chemisty of silver helps to create new ideas solving most of fundamental, biological and technical issues, which still exist in this highly competitive area, to provide important competences and practical perspectives of SERS-based devices.

The authors aknowledge support by the Russian Science Foundation (grant no. 14-13-00871) and partial support from M. V. Lomonosov Moscow State University Program of Development for providing analytical research of the materials. We appreciate help and fruitful discussions with our colleagues V. K. Ivanov, A. E. Baranchikov, A. V. Garshev, S. V. Savilov, A. S. Sarycheva and O. Sosnovtseva.

References

1 M. Burrel, J. M. Llovet, C. Ayuso, C. Iglesias, M. Sala, R. Miquel, T. Caralt, J. R. Ayuso, M. Solé, M. Sanchez, C. Brú and J. Bruix, *Hepatology*, 2003, **38**, 1034.
2 D. O. Cosgrove, *Ultrasound Med. Biol.*, 2010, **36**, 2146.
3 T. Dohmen, E. Kataoka, I. Yamada, K. Miura, S. Ohshima, T. Shibuya, D. Segawa, W. Sato, Y. Anezaki, H. Ishii, K. Kamada, T. Goto and H. Ohnishi, *Intern. Med.*, 2012, **51**, 1.
4 P. C. Sontum, *Ultrasound Med. Biol.*, 2008, **34**, 824.
5 M. Di Martino, D. Marin, A. Guerrisi, M. Baski, F. Galati, M. Rossi, S. Brozzetti, R. Masciangelo, R. Passariello and C. Catalano, *Radiology*, 2010, **256**, 806.
6 G. J. Puppels, F. F. M. de Mul, C. Otto, J. Greve, M. Robert-Nicoud, D. J. Arndt-Jovin and T. M. Jovin, *Nature*, 1990, **347**, 301.
7 B. R. Wood, P. Caspers, G. J. Puppels, S. Pandiancherri and D. McNaughton, *Anal. Bioanal. Chem.*, 2007, **387**, 1691.
8 M. Moskovits, *Rev. Mod. Phys.*, 1985, **57**, 783.
9 R. A. Alvarez-Puebla and L. M. Liz-Marzán, *Small*, 2010, **6**, 604.
10 Z. Wang, S. Pan, T. D. Krauss, H. Du and L. J. Rothberg, *Proc. Natl. Acad. Sci. USA*, 2003, **100**, 8638.
11 N. A. Brazhe, S. Abdali, A. R. Brazhe, O. G. Luneva, N. Y. Bryzgalova, E. Y. Parshina, O. V. Sosnovtseva and G. V. Maksimov, *Biophys. J.*, 2009, **97**, 3206.
12 J. Fang, S. Liu and Z. Li, *Biomaterials*, 2011, **32**, 4877.
13 G. Xu, X. Qiao, X. Qiu and J. Chen, *Rare Metal Mater. Eng.*, 2010, **39**, 1532.
14 J. N. Anker, W. P. Hall, O. Lyandres, N. C. Shah, J. Zhao and R. P. Van Duyne, *Nat. Mater.*, 2008, **7**, 442.
15 X. Wang, Y. Li, H. Wang, Q. Fu, J. Peng, Y. Wang, J. Du, Y. Zhou and L. Zhan, *Biosens. Bioelectron.*, 2010, **26**, 404.
16 J. K. Daniels and G. Chumanov, *J. Phys. Chem. B*, 2005, **109**, 17936.
17 A. März, B. Mönch, P. Rösch, M. Kiehntopf, T. Henkel and J. Popp, *Anal. Bioanal. Chem.*, 2011, **400**, 2755.
18 J. Kneipp, H. Kneipp, B. Wittig and K. Kneipp, *Nano Lett.*, 2007, **7**, 2819.
19 R. M. Jarvis and R. Goodacre, *Chem. Soc. Rev.*, 2008, **37**, 931.
20 T. A. Taton and C. A. Mirkin, *Science*, 2000, **289**, 1757.
21 X. K. Meng, S. C. Tang and S. Vongehr, *J. Mater. Sci. Technol.*, 2010, **26**, 487.
22 B. Pietrobon and V. Kitaev, *Chem. Mater.*, 2008, **20**, 5186.
23 M. Casella, A. Lucotti, M. Tommasini, M. Bedoni, E. Forvi, F. Gramatica and G. Zerbi, *Spectrochim. Acta, Part A*, 2011, **79**, 915.
24 M. S. Kiran, T. Itoh, K. Yoshida, N. Kawashima, V. Biju and M. Ishikawa, *Anal. Chem.*, 2010, **82**, 1342.
25 N. Leopold and B. Lendl, *J. Phys. Chem. B*, 2003, **107**, 5723.
26 M. Mahato, P. Pal, B. Tah, M. Ghosh and G. B. Talapatra, *Colloids Surf. B*, 2011, **88**, 141.
27 D. E. Charles, D. Aherne, M. Gara, D. M. Ledwith, Y. K. Gun'ko, J. M. Kelly, W. J. Blau and M. E. Brennan-Fournet, *ACS Nano*, 2010, **4**, 55.
28 Y. Lu, G. L. Liu, J. Kim, Y. X. Mejia and L. P. Lee, *Nano Lett.*, 2005, **5**, 119.
29 N. R. Jana and T. Pal, *Adv. Mater.*, 2007, **19**, 1761.
30 P. V. Asharani, S. Sethu, S. Vadukumpully, S. Zhong, C. T. Lim, M. P. Hande and S. Valiyaveettil, *Adv. Funct. Mater.*, 2010, **20**, 1233.
31 W. Mu, D.-K. Hwang, R. P. H. Chang, M. Sukharev, D. B. Tice and J. B. Ketterson, *J. Chem. Phys.*, 2011, **134**, 124312.
32 Z. Huang, G. Meng, Q. Huang, Y. Yang, C. Zhu and C. Tang, *Adv. Mater.*, 2010, **22**, 4136.
33 X.-Y. Zhang, A. Hu, T. Zhang, W. Lei, X.-J. Xue, Y. Zhou and W. W. Duley, *ACS Nano*, 2011, **5**, 9082.
34 L. Polavarapu, J. Pérez-Juste, Q.-H. Xu and L. M. Liz-Marzán, *J. Mater. Chem. C*, 2014, **2**, 7460.
35 R. A. Álvarez-Puebla and L. M. Liz-Marzán, *Energy Environ. Sci.*, 2010, **3**, 1011.
36 D. Cialla, A. März, R. Böhme, F. Theil, K. Weber, M. Schmitt and J. Popp, *Anal. Bioanal. Chem.*, 2012, **403**, 27.
37 C. Beer, R. Foldbjerg, Y. Hayashi, D. S. Sutherland and H. Autrup, *Toxicol. Lett.*, 2012, **208**, 286.
38 K. Chaloupka, Y. Malam and A. M. Seifalian, *Trends Biotechnol.*, 2010, **28**, 580.
39 D. D. Evanoff, Jr. and G. Chumanov, *ChemPhysChem*, 2005, **6**, 1221.
40 B. Lim and Y. Xia, *Angew. Chem. Int. Ed.*, 2011, **50**, 76.
41 B. Wiley, Y. Sun, B. Mayers and Y. Xia, *Chem. Eur. J.*, 2005, **11**, 454.
42 Q. Zhang, Y. N. Tan, J. Xie and J. Y. Lee, *Plasmonics*, 2009, **4**, 9.
43 T. Huang and X.-H. N. Xu, *J. Mater. Chem.*, 2010, **20**, 9867.
44 J. Zhang, S. A. Winget, Y. Wu, D. Su, X. Sun, Z.-X. Xie and D. Qin, *ACS Nano*, 2016, **10**, 2607.
45 S. Peng and Y. Sun, *Chem. Mater.*, 2010, **22**, 6272.
46 S. C. Boca, M. Potara, A.-M. Gabudean, A. Juhem, P. L. Baldeck and S. Astilean, *Cancer Lett.*, 2011, **311**, 131.
47 D. Yu and V. W.-W. Yam, *J. Phys. Chem. B*, 2005, **109**, 5497.
48 J. Zeng, X. Xia, M. Rycenga, P. Henneghan, Q. Li and Y. Xia, *Angew. Chem. Int. Ed.*, 2011, **50**, 244.
49 L. Fan and R. Guo, *Cryst. Growth Des.*, 2008, **8**, 2150.
50 A. Guerrero-Martínez, S. Barbosa, I. Pastoriza-Santos and L. M. Liz-Marzán, *J. Colloid Interface Sci.*, 2011, **16**, 118.
51 B. K. Jena, B. K. Mishra and S. Bohidar, *J. Phys. Chem. C*, 2009, **113**, 14753.
52 H. Liang, Z. Li, W. Wang, Y. Wu and H. Xu, *Adv. Mater.*, 2009, **21**, 4614.
53 X. S. Shen, G. Z. Wang, X. Hong and W. Zhu, *Phys. Chem. Chem. Phys.*, 2009, **11**, 7450.
54 J. H. Zhang, H. Liu, P. Zhan, Z. L. Wang and N. B. Ming, *Adv. Funct. Mater.*, 2007, **17**, 1558.
55 E. C. Cho, C. M. Cobley, M. Rycenga and Y. Xia, *J. Mater. Chem.*, 2009, **19**, 6317.
56 Y. Sun and Y. Xia, *Science*, 2002, **298**, 2176.
57 S. Coskun, B. Aksoy and H. E. Unalan, *Cryst. Growth Des.*, 2011, **11**, 4963.
58 D. Chen, X. Qiao, X. Qiu, J. Chen and R. Jiang, *Nanotechnology*, 2010, **21**, 025607.
59 H. Liang, H. Yang, W. Wang, J. Li and H. Xu, *J. Am. Chem. Soc.*, 2009, **131**, 6068.
60 X. Luo, Z. Li, C. Yuan and Y. Chen, *Mater. Chem. Phys.*, 2011, **128**, 77.
61 A. S. Sarycheva, N. A. Brazhe, A. A. Baizhumanov, E. I. Nikelshparg, A. A. Semenova, A. V. Garshev, A. E. Baranchikov, V. K. Ivanov, G. V. Maksimov, O. Sosnovtseva and E. A. Goodilin, *J. Mater. Chem. B*, 2016, **4**, 539.
62 N. A. Brazhe, A. B. Evlyukhin, E. A. Goodilin., A. A. Semenova, S. M. Novikov, S. I. Bozhevolnyi, B. N. Chichkov, A. S. Sarycheva, A. A. Baizhumanov, E. I. Nikelshparg, L. I. Deev, E. G. Maksimov, G. V. Maksimov and O. Sosnovtseva, *Sci. Rep.*, 2015, **5**, 13793.

63 A. S. Sarycheva, V. K. Ivanov, A. E. Baranchikov, S. V. Savilov, A. V. Sidorov and E. A. Goodilin, *RSC Adv*., 2015, **5**, 90335.
64 A. A. Semenova, V. K. Ivanov, A. E. Baranchikov, S. V. Savilov and E. A. Goodilin, *Funct. Mater. Lett*., 2016, **9**, 1650014-1.
65 A. A. Semenova, N. A. Brazhe, E. Y. Parshina, V. K. Ivanov, G. V. Maksimov and E. A. Goodilin, *Plasmonics*, 2014, **9**, 227.
66 A. S. Sarycheva, A. A. Semenova, E. Y. Parshina, N. A. Brazhe, A. Y. Polyakov, A. Y. Kozmenkova, A. V. Grigorieva, G. V. Maksimov and E. A. Goodilin, *Mater. Lett*., 2014, **121**, 66.
67 A. A. Semenova, V. K. Ivanov, S. V. Savilov and E. A. Goodilin, *CrystEngComm*, 2013, **15**, 7863.
68 N. A. Brazhe, E. Y. Parshina, V. V. Khabatova, A. A. Semenova, A. R. Brazhe, A. I. Yusipovich, A. S. Sarycheva, A. A. Churin, E. A. Goodilin, G. V. Maksimov and O. V. Sosnovtseva, *J. Raman Spectrosc.*, 2013, **44**, 686.
69 A. A. Semenova, E. A. Goodilin, N. A. Brazhe, V. K. Ivanov, A. E. Baranchikov, V. A. Lebedev, A. E. Goldt, O. V. Sosnovtseva, S. V. Savilov, A. V. Egorov, A. R. Brazhe, E. Y. Parshina, O. G. Luneva, G. V. Maksimov and Yu. D. Tretyakov, *J. Mater. Chem*., 2012, **22**, 24530.
70 A. A. Semenova, E. A. Goodilin and Yu. D. Tretyakov, *Mendeleev Commun*., 2011, **21**, 312.
71 E. Yu. Parshina, A. S. Sarycheva, A. I. Yusipovich, N. A. Brazhe, E. A. Goodilin and G. V. Maksimov, *Laser Phys. Lett.*, 2013, **10**, 075607.
72 Yu. D. Tretyakov and E. A. Goodilin, *Russ. Chem. Rev*., 2009, **78**, 801 (*Usp. Khim.*, 2009, **78**, 867).
73 A. A. Semenova, N. A. Braze, G. V. Maksimov, I. A. Semenova, A. P. Semenov and E. A. Goodilin, *Mendeleev Commun.*, 2016, **26**, 32.
74 X. C. Jiang, S. X. Xiong, Z. A. Tian, C. Y. Chen, W. M. Chen and A. B. Yu, *J. Phys. Chem. C*, 2011, **115**, 1800.
75 J. H. Simons, *J. Phys. Chem.*, 1932, **36**, 652.
76 J.-H. Park, *Mater. Lett*., 1990, **9**, 313.
77 L. C. Beavis, *Rev. Sci. Instrum*., 1972, **43**, 122.
78 G. Manickam, R. Gandhiraman, R. K. Vijayaraghavan, L. Kerr, C. Doyle, D. E. Williams and S. Daniels, *Analyst*, 2012, **137**, 5265.
79 R. Wiesinger, I. Martina, Ch. Kleber and M. Schreiner, *Corros. Sci*., 2013, **77**, 69.
80 L. S. Kibis, A. I. Stadnichenko, E. M. Pajetnov, S. V. Koscheev, V. I. Zaykovskii and A. I. Boronin, *Appl. Surf. Sci*., 2010, **257**, 404.
81 A. V. Sidorov, A. V. Grigorieva, A. E. Goldt, O. E. Eremina, I. A. Veselova, S.V. Savilov and E. A. Goodilin, *Funct. Mater. Lett*., 2016, **9**, 1650016.
82 A. Bayu, D. Nandiyanto and K. Okuyama, *Adv. Powder Technol.*, 2011, **22**, 1.
83 X.-H. Liu, Y.-Y. Cao, H.-Y. Peng, H.-S. Qian, X.-Z. Yang and H.-B. Zhang, *CrystEngComm*, 2014, **16**, 2365.
84 Z. Deng, M. Chen and L. Wu, *J. Phys. Chem. C*, 2007, **111**, 11692.
85 D. Radziuk, R. Schuetz, A. Masic and H. Moehwald, *Phys. Chem. Chem. Phys*., 2014, **16**, 24621.
86 M. Jasiorski, K. Łuszczyk and A. Baszczuk, *J. Alloys Compd.*, 2014, **588**, 70.
87 J. C. Flores, V. Torres, M. Popa, D. Crespo and J. M. Calderón-Moreno, *J. Non-Cryst. Solids*, 2008, **354**, 5435.
88 M. Zhu, G. Qian, Z. Wang and M. Wang, *Mater. Chem. Phys*., 2006, **100**, 333.
89 K. Wang, X. Zhang, C. Niu and Y. Wang, *ACS Appl. Mater. Interfaces*, 2014, **6**, 1272.
90 T. Liu, D. Li, D. Yang and M. Jiang, *Colloids Surf. A*, 2011, **387**, 17.
91 H. Xu, E. J. Bjerneld, M. Käll and L. Börjesson, *Phys. Rev. Lett.*, 1999, **83**, 4357.
92 N. Shaklai, J. Yguerabide and H. M. Ranney, *Biochemistry*, 1977, **16**, 5585.
93 P. Stein, J. M. Burke and T. G. Spiro, *J. Am. Chem. Soc.*, 1975, **97**, 2304.
94 R. T. Tom, A. K. Samal, T. S. Sreeprasad and T. Pradeep, *Langmuir*, 2007, **23**, 1320.
95 A. C. De Luca, G. Rusciano, R. Ciancia, V. Martinelli, G. Pesce, B. Rotoli, L. Selvaggi and A. Sasso, *Opt. Express*, 2008, **16**, 7943.
96 B. R. Wood and D. McNaughton, *J. Raman Spectrosc*., 2002, **33**, 517.
97 E. A. Vitol, Z. Orynbayeva, M. J. Bouchard, J. Azizkhan-Clifford, G. Friedman and Y. Gogotsi, *ASC Nano*, 2009, **3**, 3529.
98 L.-L. Qu, D.-W. Li, L.-X. Qin, J. Mu, J. S. Fossey and Y.-T. Long, *Anal. Chem*., 2013, **85**, 9549.
99 T.-Y. Liu, K.-T. Tsai, H.-H. Wang, Y. Chen, Y.-H. Chen, Y.-C. Chao, H.-H. Chang, C.-H. Lin, J.-K. Wang and Y.-L. Wang, *Nat. Commun.*, 2011, **2**, 538.
100 A. Sivanesan, E. Witkowska, W. Adamkiewicz, Ł. Dziewit, A. Kamińska and J. Waluk, *Analyst*, 2014, **139**, 1037.
101 G. Chandra, K. S. Ghosh, S. Dasgupta and A. Roy, *Int. J. Biol. Macromol*., 2010, **47**, 361.
102 B. Kang, L. A. Austin and M. A. El-Sayed, *ACS Nano*, 2014, **8**, 4883.
103 C. Mammucari and R. Rizzuto, *Mech. Ageing Dev*., 2010, **131**, 536.
104 C. T. Chu, J. Ji, R. K. Dagda, J. F. Jiang, Y. Y. Tyurina, A. A. Kapralov, V. A. Tyurin, N. Yanamala, I. H. Shrivastava, D. Mohammadyani, K. Z. Qiang Wang, J. Zhu, J. Klein-Seetharaman, K. Balasubramanian, A. A. Amoscato, G. Borisenko, Z. Huang, A. M. Gusdon, A. Cheikhi, E. K. Steer, R. Wang, C. Baty, S. Watkins, I. Bahar, H. Bayır and V. E. Kagan, *Nat. Cell Biol*., 2013, **15**, 1197.
105 M. P. Murphy, *Biochem. J.*, 2009, **417**, 1.
106 E. T. Chouchani, C. Methner, S. M. Nadtochiy, A. Logan, V. R. Pell, S. Ding, A. M. James, H. M. Cochemé, J. Reinhold, K. S. Lilley, L. Partridge, I. M. Fearnley, A. J. Robinson, R. C. Hartley, R. A. J. Smith, T. Krieg, P. S. Brookes and M. P. Murphy, *Nat. Med*., 2013, **19**, 753.
107 J. D. Cortese and C. R. Hackenbrock, *Biochim. Biophys. Acta*, 1993, **1142**, 194.
108 J. D. Cortese, A. L. Voglino and C. R. Hackenbrock, *Biochim. Biophys. Acta*, 1995, **1228**, 216.
109 F. Adar and M. Erecinska, *FEBS Lett*., 1977, **80**, 195.
110 S. Berezhna, H. Wohlrab and P. M. Champion, *Biochemistry*, 2003, **42**, 6149.
111 N. A. Brazhe, M. Treiman, A. R. Brazhe, N. L. Find, G. V. Maksimov and O. V. Sosnovtseva, *PLoS One*, 2012, **7**, e41990.
112 N. A. Brazhe, M. Treiman, B. Faricelli, J. H. Vestergaard and O. Sosnovtseva, *PLoS One*, 2013, **8**, e70488.
113 M. Okada, N. I. Smith, A. F. Palonpon, H. Endo, S. Kawata, M. Sodeoka and K. Fujita, *Proc. Natl. Acad. Sci. USA*, 2012, **109**, 28.
114 W. T. Borden and E. R. Davidson, *J. Am. Chem. Soc*., 1980, **102**, 7960.
115 L. Chen, X. Han, J. Yang, J. Zhou, W. Song, B. Zhao, W. Xu and Y. Ozaki, *J. Colloid Interface Sci*., 2011, **360**, 482.
116 Ö. F. Karataş, E. Sezgin, Ö. Aydın and M. Çulha, *Colloids Surf., B*, 2009, **71**, 315.
117 R. Böhme, M. Mkandawire, U. Krause-Buchholz, P. Rösch, G. Rödel, J. Popp and V. Deckert, *Chem. Commun.*, 2011, **47**, 11453.
118 D. K. Lim, K. S. Jeon, J. H. Hwang, H. Kim, S. Kwon, Y. D. Suh and J. M. Nam, *Nat. Nanotechnol*., 2011, **6**, 452.
119 S. Zong, C. Chen, Z. Wang, Y. Zhang and Y. Cui, *ACS Nano*, 2016, **10**, 2950.
120 E. A. Vitol, Z. Orynbayeva, G. Friedman and Y. Gogotsi, *J. Raman Spectrosc.*, 2012, **43**, 817.
121 S. R. Panikkanvalappil, M. A. Mahmoud, M. A. Mackey and M. A. El-Sayed, *ACS Nano*, 2013, **7**, 7524.
122 J. C. Fraire, L. A. Pérez and E. A. Coronado, *ACS Nano*, 2012, **6**, 3441.
123 C. Costas, V. López-Puente, G. Bodelón, C. González-Bello, J. Pérez-Juste, I. Pastoriza-Santos and L. M. Liz-Marzán, *ACS Nano*, 2015, **9**, 5567.
124 W. Kim, Y.-H. Kim, H.-K. Park and S. Choi, *ACS Appl. Mater. Interfaces*, 2015, **7**, 27910.
125 J. Lee, Q. Zhang, S. Park, A. Choe, Z. Fan and H. Ko, *ACS Appl. Mater. Interfaces*, 2016, **8**, 634.
126 E. A. Vitol, G. Friedman and Y. Gogotsi, *J. Nanosci. Nanotechnol*., 2014, **14**, 3046.
127 E. A. Vitol, E. Brailoiu, Z. Orynbayeva, N. J. Dun, G. Friedman and Y. Gogotsi, *Anal. Chem.*, 2010, **82**, 6770.

Received: 14th March 2016; Com. 16/4870